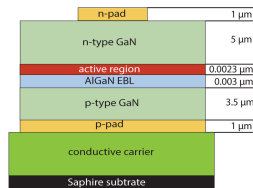


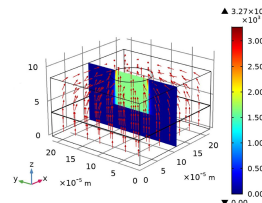
Three-Dimensional Numerical Study on the Efficiency Droop in InGaN/GaN Light-Emitting Diodes

Volume 11, Number 1, February 2019

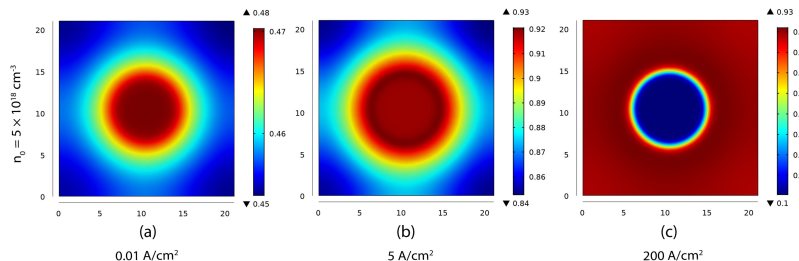
Quoc-Hung Pham
 Jyh-Chen Chen
 Huy-Bich Nguyen



Schematic diagram of an SWQ LED showing the layer composition



Electron current density at the center of the LED chip on the y - z plane at 200 A/cm^2 for $n_i = 5 \times 10^{18} \text{ cm}^{-3}$



Local IQE at the active layer with various injection current densities for $n_e = 5 \times 10^{18} \text{ cm}^{-3}$

DOI: 10.1109/JPHOT.2019.2893198

1943-0655 © 2019 IEEE

Three-Dimensional Numerical Study on the Efficiency Droop in InGaN/GaN Light-Emitting Diodes

Quoc-Hung Pham ¹, Jyh-Chen Chen ¹, and Huy-Bich Nguyen²

¹Department of Mechanical Engineering, National Central University, Jhongli City 32001, Taiwan

²Department of Mechanical Engineering, Nong Lam University, Ho Chi Minh City, Vietnam

DOI:10.1109/JPHOT.2019.2893198

1943-0655 © 2018 IEEE. Translations and content mining are permitted for academic research only. Personal use is also permitted, but republication/redistribution requires IEEE permission. See http://www.ieee.org/publications_standards/publications/rights/index.html for more information.

Manuscript received December 7, 2018; revised December 31, 2018; accepted January 10, 2019. Date of publication January 16, 2019; date of current version February 8, 2019. This work was supported by the Ministry of Science and Technology of Taiwan (MOST), R.O.C., under Grant MOST 104-2221-E-008-079 -MY3. Corresponding author: Jyh-Chen Chen (e-mail: jchen@cc.ncu.edu.tw).

Abstract: The efficiency droop characteristics of single quantum well (SQW) InGaN/GaN light-emitting diodes (LEDs) including the phase-space filling (PSF) effect are predicted by a three-dimensional (3-D) numerical simulation. The carrier transport is based on the solution of the 3-D non-linear Poisson and drift-diffusion equations for both holes and electrons. A modified formulation of the Shockley—Reed—Hall (SRH) coefficient is proposed to describe the SRH carrier lifetime behavior, which increases at a low excitation level and decreases at a higher one. The current crowding causes a non-uniform distribution of the carrier concentration in the active layer that leads to the inversion of the local internal quantum efficiency (IQE) under the n-pad region when the injection current density increases from low to high levels. To further understand the correlation of the efficiency droop with the PSF effect, we systematically investigate carrier transport in the SQW InGaN/GaN LEDs and how the different PSF effect coefficients affect the current–voltage curve and IQE. The lumped IQE found in this study agrees well with previous experimental measurements. Moreover, the PSF effect has a strong impact on the IQE behavior including its peak and droop in efficiency.

Index Terms: InGaN/GaN, light-emitting diodes (LEDs), optoelectronic devices, phase space filling (PSF) effect, current spreading.

1. Introduction

LEDs have found numerous applications in visual displays and sensing devices, as well as for illumination and general lighting and communication technology. Their advantages include their small size, long lifetime, high efficiency and low energy consumption. The high-power GaN-based LEDs are considered to hold great promise for development as a new lighting source to replace traditional lighting devices. However, some challenges remain to be overcome. One of the most significant problems for InGaN/GaN-based LEDs is the efficiency droop at higher injected carrier densities, which causes a reduction in the internal quantum efficiency (IQE) [1], [2]. The efficiency droop has been explained as due to internal non-radiative loss and electron leakage. The internal non-radiative losses include Auger recombination [3], reduced active volume effects [4] and carrier delocalization [5], [6]. Some studies have shown that Auger recombination could be the major

contributor to the droop in the IQE [7]–[9]. The occurrence of electron leakage outside the active region could be caused by various mechanisms such as the quantum confined Stark effect (QCSE) resulting in polarization sheet charges at the electron blocking layer (EBL)/spacer and quantum well (QW)/ quantum barrier (QB) interfaces [1], poor hole injection [10], [11], asymmetry in the electron and hole active doping concentrations and in the carrier transport parameters [12], current crowding [13], electron overflow [14], defect-assisted tunneling [15] or radiative recombination saturation [16]. Up to now, though, the actual reason for the efficiency droop has not yet been conclusively determined.

The efficiency droop in LEDs is often described by the ABC model [4], [9], [17]–[20]. In this model, the recombination process is described by means of $An + Bnp + Cn^2p$, where A , B , and C are constants, and n and p indicate the electron and hole density, respectively, and the terms An , Bnp and Cn^2p represent the Shockley-Read-Hall recombination (SRH), radiative and Auger recombination, respectively. The hole and electron densities are assumed to be equal in the ABC model. The variation of the ABC coefficients with the carrier density and the physical insight of the carrier leakage are hidden in the ABC model fitting procedure.

One potential explanation for the efficiency droop in InGaN/GaN LEDs is the PSF effect [21], [22], which represents the influence of the Fermi-Dirac carrier statistics on the recombination processes [23], [24]. It can be used to explain the reduction of the radiative recombination that leads to the efficiency droop at high carrier densities [17]. The PSF effect also has a strong impact on the peak IQE and the efficiency droop in the LEDs. A strong PSF effect can be found in c-plane LEDs, while a weaker PSF effect can be discovered in semi-polar/non-polar LEDs [17]. A modified ABC model [18] is proposed where B and C are not considered to be constants but the PSF effect is included. In SRH recombination, the An term in the ABC model is considered to have a weak effect on the efficiency droop because it makes only a first order of magnitude contribution to the total recombination processes. Recently, non-radiative SRH recombination has also been found to produce non-radiative recombination centers in QWs that show a super-linear increase in the density [22] thereby dominating the total recombination process [25] under higher injected carrier rates. This can also be explained as due to the electrons occupying the higher energy states having a much higher probability of being captured by non-radiative SRH recombination. SRH recombination has a strong effect on the peak efficiency and the efficiency droop in InGaN/GaN LEDs. These ideas have recently been confirmed by numerical simulation and experimental measurements [26]. Wang *et al.* [22] used the self-consistent solution of the Schrödinger-Poisson equations to estimate the extended carrier SRH coefficient $A(k_r)$ as a function of the in-plane wave vector k_r arising from the PSF effect. Thus, the PSF effect should be considered in the SRH recombination coefficient, also known as the inversion of the SRH carrier lifetime. Several studies have shown that the SRH carrier lifetime varies with the carrier density in the InGaN/GaN MQW LEDs [18], [19], InGaN/GaN double-heterostructure LEDs [23] and GaAs/Al_{0.3}Ga_{0.7}As heterojunctions [27]. Based on the ABC model, the SRH carrier lifetime decreases with an increase of the carrier density [23]. However, some studies have shown the opposite tendency [28], [29]. Okur *et al.* [28] measured the internal quantum efficiencies (IQE) and carrier lifetimes of semi-polar InGaN/GaN LEDs using temperature-dependent, carrier-density-dependent, and time-resolved photoluminescence. Their results showed the SRH carrier lifetime to be lowest at low excitation levels, increasing as the excitation level rises due to the saturation of non-radiative centers. The same tendency was also obtained by Walker *et al.* [29] for double hetero-structures composed of III-V semiconductors which were measured by a power-dependent relative photoluminescence method. Langer *et al.* [30] studied the carrier lifetimes of single GaInN/GaN QW structures by time-resolved photoluminescence spectroscopy. In contrast to the common treatment of the SRH carrier lifetime, their results show that the SRH carrier lifetime increases at a low excitation level and decreases at a higher one. They calculated the non-radiative lifetimes based on the background carrier density [31], [32]. However, they did not take into account the reduction of the SRH carrier lifetime at high injection levels.

It has been identified in both theoretical and experimental work that the Auger recombination, a three-particle electron-electron-hole (eeh) or hole-hole-electron (hhe) carrier-carrier interaction,

causes an efficiency droop in InGaN/GaN LEDs [3], [23], [33]. In contrast, it is the leakage of electrons that are not captured by the QWs into the EBL or p-doped LED layers, carrier leakage by thermionic emission, that causes the efficiency droop in the InGaN/GaN LEDs [1], [10]–[16]. The efficiency droop is strongly dependent on the device design and relates to many factors such as the QCSE, poor hole injection, asymmetry of the electron and hole doping profiles, current crowding, defect-assisted tunneling and radiative recombination saturation [1], [10]–[16] rather than being caused by a single mechanism. Although Auger recombination and electron leakage are different physical processes, they actually interact together. Theoretical calculations [34] and experimental evidence [8], [9] confirm that the occurrence of Auger recombination will assist electron leakage, also known as direct carrier leakage. Auger recombination generates hot carriers that can be recaptured by the QWs or facilitate electron leakage outside the QWs, as has been found to occur in GaInAsP/InP double-heterostructure LEDs and lasers [35], InGaN/GaN QW(s) blue LEDs [7] and SQW blue LEDs [36].

Current crowding has been identified as one reason for the efficiency droop [13], because it enhances the local carrier densities, leading to an increase in electron leakage. A two-dimensional (2D) model for solving the drift-diffusion and Poisson equations [13] has been developed which does explain the occurrence of current crowding and development of radiative recombination regions. However, the current density distribution inside an LED chip is actually three-dimensional (3D), therefore, a 3D simulation is needed to provide deeper information about the current density distribution and the distribution of local carrier densities inside the LED chip, to obtain a better understanding of their influence on the IQE behavior. In this study, we use the 3D non-linear Poisson and drift-diffusion equations to calculate the carrier transport. The 3D drift-diffusion and Poisson equations are solved based on Fermi-Dirac statistics to clarify the local behavior of the carrier densities and the radiative and non-radiative recombination. From the Shockley-Read-Hall recombination theory [31], [32], a modified formula is proposed for the SRH lifetime which takes into account the influence of the PSF which depends on the carrier density in the active layer. In this formula, the SRH recombination lifetime increases with the carrier density at low injection levels and decreases at higher injection levels. All recombination processes are considered, with both electron and hole densities. The PSF effect is included in all recombination processes. The influence of the non-uniform current distribution in the chip on the carrier density deviation in the active region leads to the change in radiative and non-radiative recombination. The variation of the local IQE with the injected carrier density is investigated to identify the droop behavior. The lumped IQE in the active region is calculated and compared with previous experimental results obtained using an actual blue light InGaN/GaN SQW LED [37].

2. Physical Modelling and Numerical Method

A schematic diagram of the vertical structure of a c-plane InGaN/GaN SQW LED as investigated by Galler *et al.* [37], [38] which is also used in the present study is shown in Fig. 1. The LED chip area is $300\text{-}\mu\text{m} \times 300\text{-}\mu\text{m}$ and the area of the active layer is $212\text{-}\mu\text{m} \times 212\text{-}\mu\text{m}$. The thicknesses of the p-pad, p-GaN, $\text{Al}_{0.1}\text{Ga}_{0.9}\text{N}$ EBL, active region, n-GaN and n-pad layer are $1\ \mu\text{m}$, $3.5\ \mu\text{m}$, $0.003\ \mu\text{m}$, $0.0023\ \mu\text{m}$, $5\ \mu\text{m}$ and $1\ \mu\text{m}$, respectively. The active region includes a 3-nm-thick $\text{In}_{0.19}\text{Ga}_{0.81}\text{N}$ SQW sandwiched between two 10-nm-thick GaN barrier layers. The thickness and In composition of the QW layer correspond to the peak emission wavelength of around 450 nm. The doping concentrations of the p-GaN, n-GaN and EBL layer are set to $2 \times 10^{19}\ \text{cm}^{-3}$, $6 \times 10^{17}\ \text{cm}^{-3}$ and $2 \times 10^{19}\ \text{cm}^{-3}$, respectively [7]. The QW layer and barrier layers are un-doped. The radius of the circular shape formed by the n-type electrode on the surface of the n-GaN is $40\ \mu\text{m}$ [38]. A p-type electrode is placed between the conductive carrier and the p-GaN and covers the entire bottom surface area of the p-GaN. The conductive carrier and sapphire substrate layers added to the chip are there to ensure de-heating and mechanical stability of the LED device and do not affect the electrical characteristics of the LED chip. Therefore, they are not considered in this study.

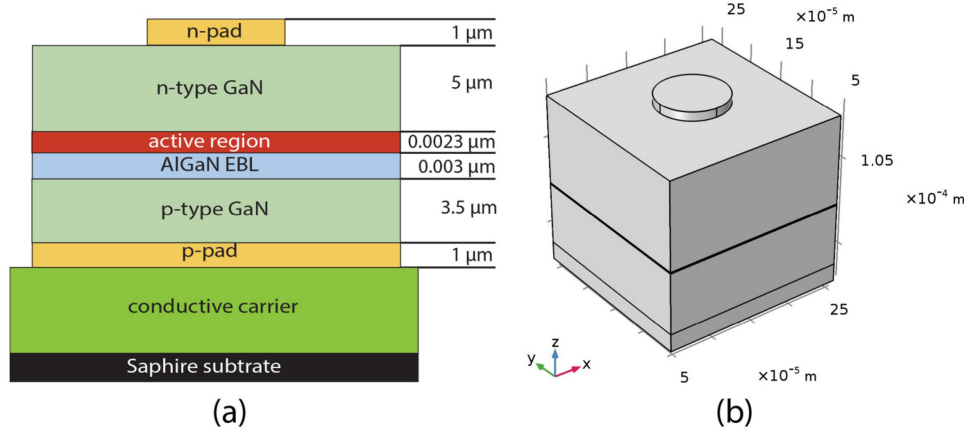


Fig. 1. Schematic diagram of an SWQ LED showing the (a) layer composition and (b) whole 3D structure.

The nonlinear 3D non-linear Poisson and drift-diffusion equations based on the Fermi-Dirac distribution are

$$\nabla^2 V = (n - p + N_A^- - N_D^+) / \varepsilon; \quad (1)$$

$$J_n = -\mu_n n \nabla V + q D_n \nabla n; \quad (2)$$

$$J_p = -\mu_p p \nabla V + q D_p \nabla p; \quad (3)$$

$$\nabla \cdot J_{n,p} = R_{SRH} + R_{rad} + R_{Auger} + R_{lk}, \quad (4)$$

where V is the band potential; ε is the material dielectric permittivity; n and p are the carrier concentrations of the electrons and holes, respectively; N_A^- and N_D^+ are the activated doping densities of the acceptor and the donor; J_n and J_p are the electron and hole current densities; and μ_n and μ_p are the mobility of electrons and holes, respectively. Here, R_{srh} , R_{rad} , R_{Auger} and R_{lk} are the SRH recombination, radiative recombination, Auger recombination and the total carrier leakage rate, respectively. The total carrier leakage rate includes the direct carrier leakage assisted by Auger recombination and the carrier leakage generated by thermionic emission. The rate recombination of electrons and holes is assumed to be equal in this study. Polarization causes deformation of the quantum wells accompanied by an electrostatic field known as QCSE. Due to the thin thicknesses of the active layer, the barrier layers and the EBL, the polarization leads to a sheet charge density between these interfaces. The polarization charge does not appear in the Poisson equation because of the existence of dipoles. The electric displacement field D at the interface boundary is affected by the condition $(D_1 - D_2) \cdot \hat{n} = \sigma_p$ [39].

The recombination rate R_{SRH} is given by the following equation [13]:

$$R_{SRH} = (pn - n_i^2) / \left(\tau_n \left[p + n_i e^{(E_i - E_t)/k_B T} \right] + \tau_p \left[n + n_i e^{(E_t - E_i)/k_B T} \right] \right), \quad (5)$$

where T is the lattice temperature; k_B is the Boltzmann's constant; E_t is the mid-gap energy level; and E_i and n_i represent the intrinsic energy level and intrinsic carrier density, respectively. The SRH recombination coefficients for holes and electrons are τ_p and τ_n , respectively. An increase of the SRH carrier lifetime in the Au-doped silicon power device is used to verify the SRH model [40]. The SRH carrier lifetime is given by [30]–[32], [40]

$$\tau_{SRH} = \tau_{p0} + \frac{\tau_{n0}}{1 + (N_0/n)}, \quad (6)$$

where $\tau_{p0, n0}$ indicates the carrier lifetime at very low injected carrier densities; N_0 is the background electron density. A similar tendency is found in InGaIn/GaN QWs in the regime between the low and high injection levels [30]. At a higher injection level, a reduction of the SRH carrier lifetime is

observed [30]. The SRH carrier lifetime calculated by equation (6) is saturated at a higher injection level. Hence, it cannot be used to predict the decrease at a higher injection level. Moreover, the SRH carrier lifetime decreases with the carrier density due to the PSF effect in InGaN/GaN QW [22]. Therefore, the empirical formulation for the SRH carrier lifetime that includes PSF effect can be modified as follows:

$$\tau_{SRH} = \tau_{p0} \frac{1}{1 + (p/n_0)} + \frac{\tau_{n0}}{1 + (N_0/n)^\gamma} \frac{1}{1 + (n/n_0)}, \quad (7)$$

where n_0 is the PSF effect coefficient; γ is a dimensionless exponent which can be determined from experimental IQE measurements. The PSF effect coefficient is in the range of $1 \times 10^{17} \text{ cm}^{-3}$ to $1 \times 10^{20} \text{ cm}^{-3}$ [17], [19], [41]. In this study, the PSF coefficient is varied from $5 \times 10^{18} \text{ cm}^{-3}$ to $5 \times 10^{19} \text{ cm}^{-3}$. The terms $\tau_{n0}/(1 + (n/n_0))$ and $\tau_{p0}/(1 + (p/n_0))$ indicate the carrier lifetimes with the PSF effect for electrons and holes, respectively. At a low injection level, $n/n_0 \ll 1$ and $p/n_0 \ll 1$ and therefore the effect of PSF is minimum. The PSF effect becomes significant when the carrier density is close to the PSF effect coefficient. By including these terms in the formula for the SRH carrier lifetime, equation (7) is able to handle the decrease of the SRH carrier lifetime with the carrier density at higher injection levels. The background doping density of the quantum well is assumed to be due to the electron presence. The SRH carrier lifetime is very sensitive to lattice and structural defects and impurities in the material, which are related to the crystal growth process [42]. The derivation of the SRH rate is based on the following assumptions: a negligible impurity concentration; a non-degenerate semiconductor; a single defect level at a stable energy position; and a much larger reemission time than the relaxation time for captured carriers [43]. However, it should be noted that the impurity concentration can increase the SRH recombination rate in InGaN/GaN MQWs [44]. This means that an increase in the impurity concentration leads to a reduction of the SRH carrier lifetime. Therefore, the term γ is included in equation (7) to overcome the uncertainty arising from structural defects and material impurities. The background electron density is selected to be $1 \times 10^{17} \text{ cm}^{-3}$, and $\gamma = 0.4$ is chosen to match the experimental IQE characteristics. From the experimental measurements, it is found that the carrier lifetime at very low injected carrier densities varies from $1 \times 10^{-6} \text{ s}$ to $5 \times 10^{-9} \text{ s}$ [3], [4], [33], [45], [46]. This is usually extracted by the ABC model in the LEDs with the assumption that the electron carrier lifetime is equal to the hole carrier lifetime. However, the carrier lifetimes of electrons and holes should be different due to the difference in the capture rate for electrons and holes at the recombination center [47]. The electron carrier lifetime is usually found to be larger than the hole carrier lifetime with the ratio of the electron carrier lifetime to the hole carrier one being 1 to 3 [40], [47], [48]. The value of parameter $\tau_{p0} = 0.1 \times 10^{-7} \text{ s}$ was found in a MQW LED that has a 3-nm-thick $\text{In}_{0.19}\text{Ga}_{0.81}\text{N}$ [49]. This value of parameter τ_{p0} is selected in this study because the material used for the active layer is the same. The value of parameter τ_{n0} is selected to be $0.15 \times 10^{-7} \text{ s}$ to match the experimental IQE characteristics.

The radiative recombination rate [50] can be formulated as follows:

$$R_{Rad} = B(np - n_i^2), \quad (8)$$

where B is the radiative coefficient. During the radiative recombination process, an electron-hole pair recombines together and then emits a photon. The empirical formulation for the radiative coefficient based on electron density proposed by David *et al.* [23] is:

$$B = \frac{B_0}{1 + (n/n_0)}. \quad (9)$$

This formula only corrects for when electron and hole densities are assumed to be equal. In this study, the electron and hole densities are not the same because of the differences in their carrier transport levels, which are decided based on the different doping profiles of p- and n-GaN and the mobility of the electrons and holes. Therefore, considering the different electron and hole densities,

equation (9) is reformulated as follows:

$$B = \frac{B_0}{1 + (np/n_0^2)}, \quad (10)$$

where B_0 is the low-density limit of the coefficient. The value of B is in the range of 1×10^{-11} to $1.5 \times 10^{-9} \text{ cm}^3 \cdot \text{s}^{-1}$ [51], [52]. The value of parameter B_0 can be selected to be $3.01 \times 10^{-10} \text{ cm}^3 \cdot \text{s}^{-1}$.

The Auger recombination rate [7] can be formulated as follows:

$$R_{Auger} = C_n(n^2p - n_i^2) + C_p(np^2 - n_i^2), \quad (11)$$

where $C_{n,p}$ indicates the Auger coefficients for holes and electrons. The empirical formulation for the Auger coefficient as proposed by David *et al.* [23] is

$$C_n = \frac{C_{n0}}{1 + (n/n_0)}, \quad (12)$$

$$C_p = \frac{C_{p0}}{1 + (p/n_0)}, \quad (13)$$

where C_0 is the low-density limit of the coefficient. The value of $C_{n,p}$ is in the range of $1.4 \text{ cm}^6/\text{s}$ to $3.0 \times 10^{-31} \text{ cm}^6/\text{s}$ [41], [45]. The value of parameter $C_{n0,p0}$ is selected to be $2.2 \times 10^{-30} \text{ cm}^6 \cdot \text{s}^{-1}$ in this study.

Since the LED structures in this study have high p-doping profiles, the main current leakage is generated by hot-carriers from the Auger process, known as direct carrier leakage, which occurs in the active layer for both electrons and holes due to the transfer of energy to a third carrier during the Auger recombination process. The Auger carrier leakage model proposed by Römer *et al.* [34] is used here. The direct carrier leakage rate can be described by

$$R_{lk,n}^{Auger} = C_{lk,n}(n^2p - n_i^2) \quad (14)$$

and

$$R_{lk,p}^{Auger} = C_{lk,p}(np^2 - n_i^2), \quad (15)$$

for electrons and holes, respectively. The Auger carrier leakage coefficients can be formulated as $C_{lk,n,p} = l^2 C_{n,p}$. l is assumed to be equal to the well thickness, without regard to units [34]. The other carrier leakages by thermionic emission, $R_{lk,n,p}^{th}$, are the electron and hole leakages which overflow out of the active layer into the p and n-GaN layers, respectively. However, hole leakage is neglected in this study due to the low hole mobility and high p-doping profile. The electron leakage rate can be calculated from the recombination rate outside the active layer. The local IQE is defined as the percentage of the radiative recombination rate over the total recombination rate as follows:

$$IQE_{sr} = R_r / (R_r + R_{SRH} + R_{Au} + R_{lk}). \quad (16)$$

The radiative and non-radiative recombination current can be obtained by integrating the distributions of the radiative and non-radiative recombination rate over the entire SQW active layer. The lumped IQE is the percentage of the total radiative recombination current over the total injection current as defined by

$$IQE = I_r / (I_{total}), \quad (17)$$

where I_r is the total radiative recombination current; and I_{total} is the total injection current.

The Poisson and drift-diffusion equations are solved using the Finite Element Method (FEM) developed by COMSOL Multiphysics. Pentahedral (square pyramidal) elements are selected for each layer of the entire chip. Convergence testing of the entire LED chip is performed using different numbers of elements: 154096, 331412, and 503902. The simulation results for the band potential, electron concentration and hole concentration for 331412 are almost the same as for 503902. To save on computational memory and computation time, the number of finite elements

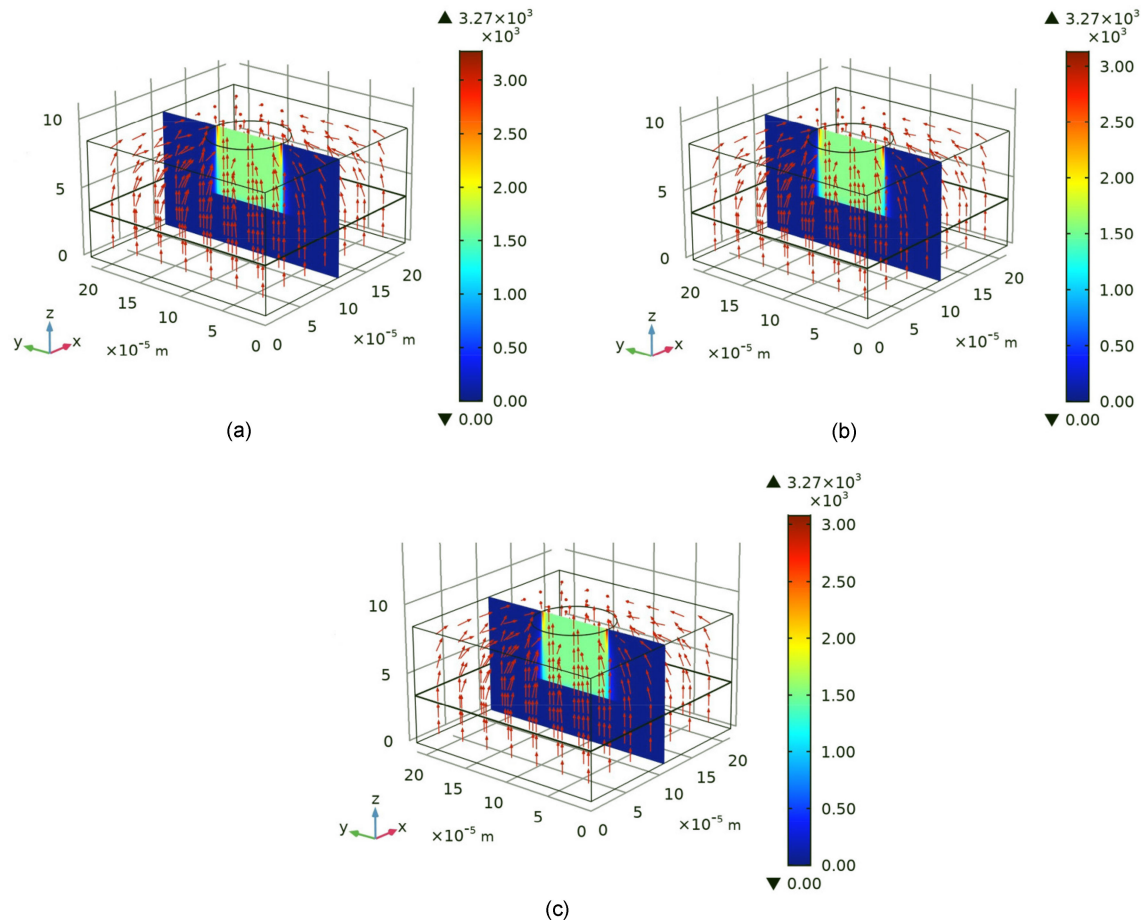


Fig. 2. Electron current density A/cm^2 at the center of the LED chip on the y - z plane and current density vector A/m^2 for the entire chip at an injection current density of $200 A/cm^2$ for various cases: (a) $n_0 = 5 \times 10^{18} cm^{-3}$, (b) $n_0 = 1 \times 10^{19} cm^{-3}$ and (c) $n_0 = 5 \times 10^{19} cm^{-3}$.

is chosen to be 331412 for the entire LED chip. The relative tolerance is 1×10^{-5} for the band potential, electron, and hole density variables.

3. Results

There are several mechanisms which might affect the PSF effect such as the quantum-confined Stark effect (QCSE), carrier lifetime, carrier transport, band structure and lattice temperature [17], [19]. The PSF effect is found to occur in the c-plane LED due to the higher carrier density ($n_0 = 1 \times 10^{18} cm^{-3}$) [17]. Weak PSF effects of $n_0 = 1 \times 10^{20} cm^{-3}$ and $n_0 = 2.4 \times 10^{19} cm^{-3}$ are also found in c-plane LEDs [41], [53], where n_0 is not so precisely known. For c-plane LEDs, the PSF coefficient varies from $1 \times 10^{17} cm^{-3}$ to $1 \times 10^{20} cm^{-3}$ [17], [19], [41]. To understand the influence of the PSF effect in c-plane LEDs, in this study, n_0 is selected to be from $5 \times 10^{18} cm^{-3}$ to $5 \times 10^{19} cm^{-3}$.

The current crowding effect is another important mechanism in real LED devices. In the present 3D simulation, current crowding can be clearly observed at high current injection rates. The average injection current density is defined as the ratio between the injection current and the cross-sectional area of the active layer. Fig. 2 shows the electron current density at the center of the LED chip on the y - z plane and current density vector for the entire chip at an injection current density of $200 A/cm^2$.

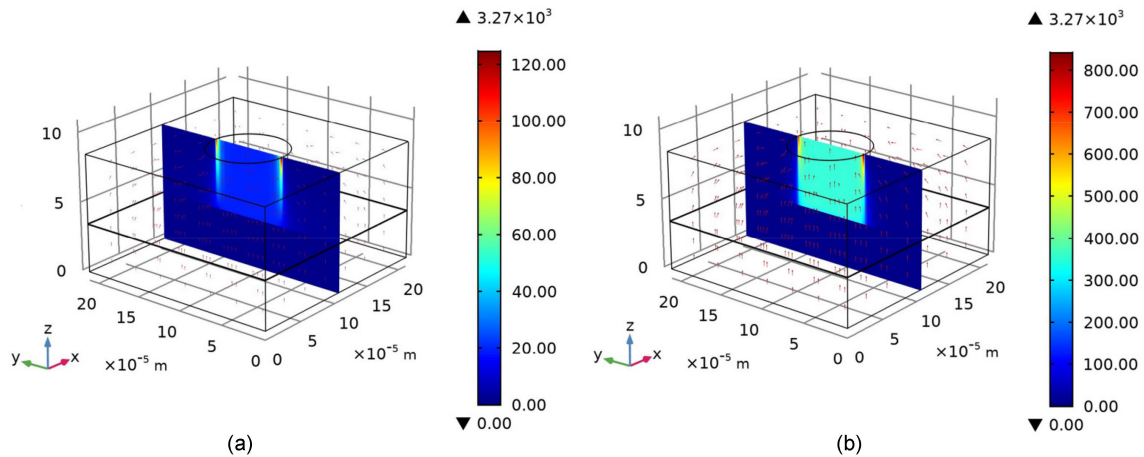


Fig. 3. Electron current density A/cm^2 at the center of the LED chip on the y - z plane and current density vector A/cm^2 for the entire chip at various injection current densities: (a) $5 A/cm^2$ and (b) $50 A/cm^2$ for the case of $n_0 = 5 \times 10^{18} cm^{-3}$.

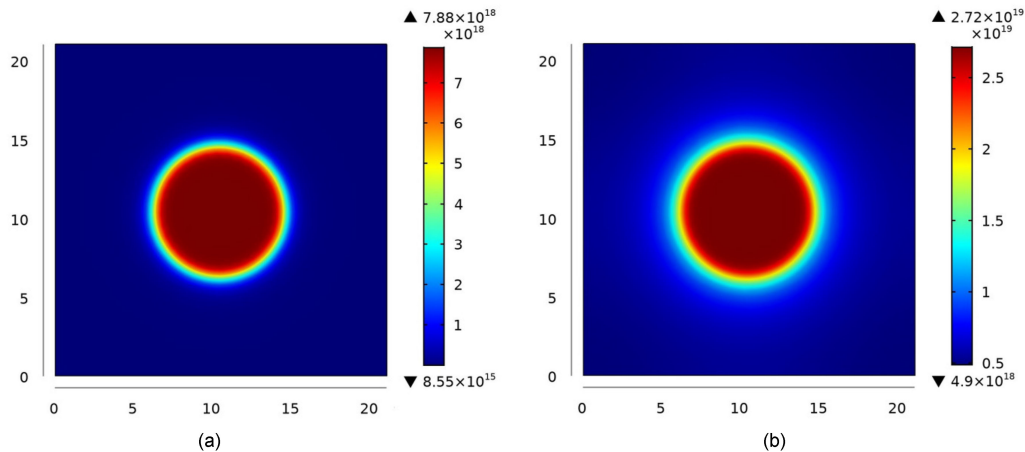


Fig. 4. Local distributions of the: (a) electron and (b) hole concentration cm^{-3} at the active layer of the LED chip with an average injection current of $200 A/cm^2$ for $n_0 = 5 \times 10^{18} cm^{-3}$.

The electron current density distribution is not uniform throughout the y - z plane. There is severe current crowding in the region under the n -pad. This will generate a non-uniform distribution in the carrier density which in turn results in non-uniformity of the local IQE. In addition, the intense photon emission from the active region under the n -pad absorbed by the n -pad causes a significant droop in the light extraction efficiency (LEE) [54]. The maximum electron current density occurs near the edge of the n -pad due to the singularity of the electric field at the metal-semiconductor interface [13], [55], [56]. With a rising n_0 , the results show a decrease in the maximum value of the current density. The current density is the highest when the PSF effect is the strongest ($n_0 = 5 \times 10^{18} cm^{-3}$). Obviously, current crowding will be weaker in cases where the PSF effect is less.

Figure 3 shows the electron current density at the center of the LED chip on the y - z plane and the current density vector for the entire chip at various injection current densities of $5 A/cm^2$ and $50 A/cm^2$ for the case of $n_0 = 5 \times 10^{18} cm^{-3}$. With the rising of the injection current density, the maximum value of the increase in the current density is shown in Fig. 3. There is a sharp difference in the magnitude of the current density in the region under the n -pad and in the outside region, when the injection current density increases.

The local electron and hole concentrations in the active layer are shown in Fig. 4. From Fig. 2, it can be clearly seen that the carrier flow from the n -pad to the p -pad and the current density

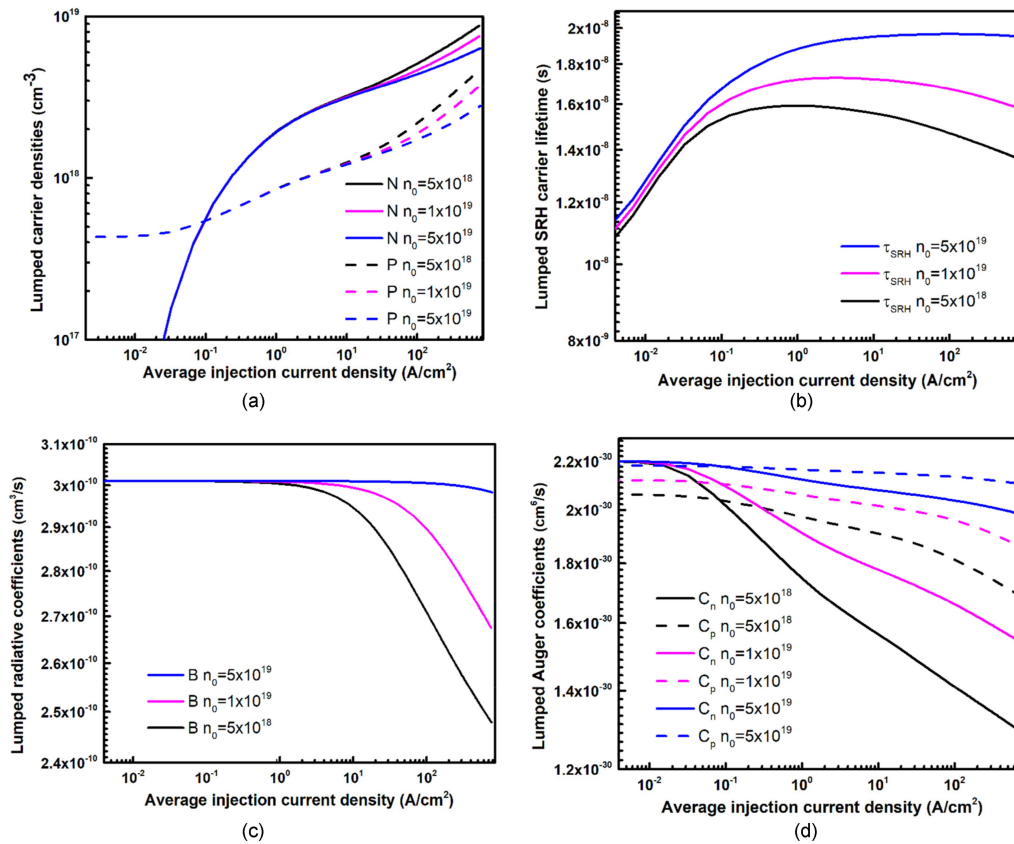


Fig. 5. (a) Lumped carrier density, (b) lumped SRH carrier lifetime, (c) lumped radiative coefficient and (d) lumped Auger coefficient versus the average injection current density A/cm^2 of the SWQ LEDs.

distribution are quite non-uniform on the y - z plane. The carrier density distributions at the active layer are affected by the current crowding effect. When the average injection current density is $200 A/cm^2$, the distributions of the electron and hole densities in the active layer are quite non-uniform, as shown in Figs. 4(a) and (b), respectively. There is carrier density crowding at the center region under the n-pad. The reason is that the carrier current prefers flowing through the lowest path of resistance between the n- and p-pads [13].

The lumped carrier density is defined as the average carrier density in the active layer volume. The lumped carrier density in the active layer versus the average injection current density is shown in Fig. 5(a). The hole densities are higher than the electron densities at low injection levels due to the higher doping profile of the p-GaN layer compared to the n-GaN layer, since the carrier currents through the active layer are mainly driven by the diffusion process. With the higher doping profile of the p-GaN layer compared to the n-GaN layer, more holes are moved to the active layer by the diffusion process in this regime. After $0.01 A/cm^2$, the electron densities in the active layer are higher than the hole densities, because the carrier current is dominated by the drift process. More electrons are shifted into the active layer by increasing the electric field to become the major carriers in the active layer. The carrier densities of both electrons and holes are not affected by the PSF effect before $1 A/cm^2$. After that, the results show a decrease in the value of the carrier density when n_0 increases from $5 \times 10^{18} cm^{-3}$ to $5 \times 10^{19} cm^{-3}$.

The SRH carrier lifetime, radiative and Auger coefficients are determined by Eqs. (7), (10), (12) and (13), respectively. The lumped recombination coefficients in the active layer versus the average injection current density are shown in Fig. 5(b), (c) and (d), respectively, and are defined as the average recombination coefficients in the active layer. The lumped SRH carrier lifetime is quite

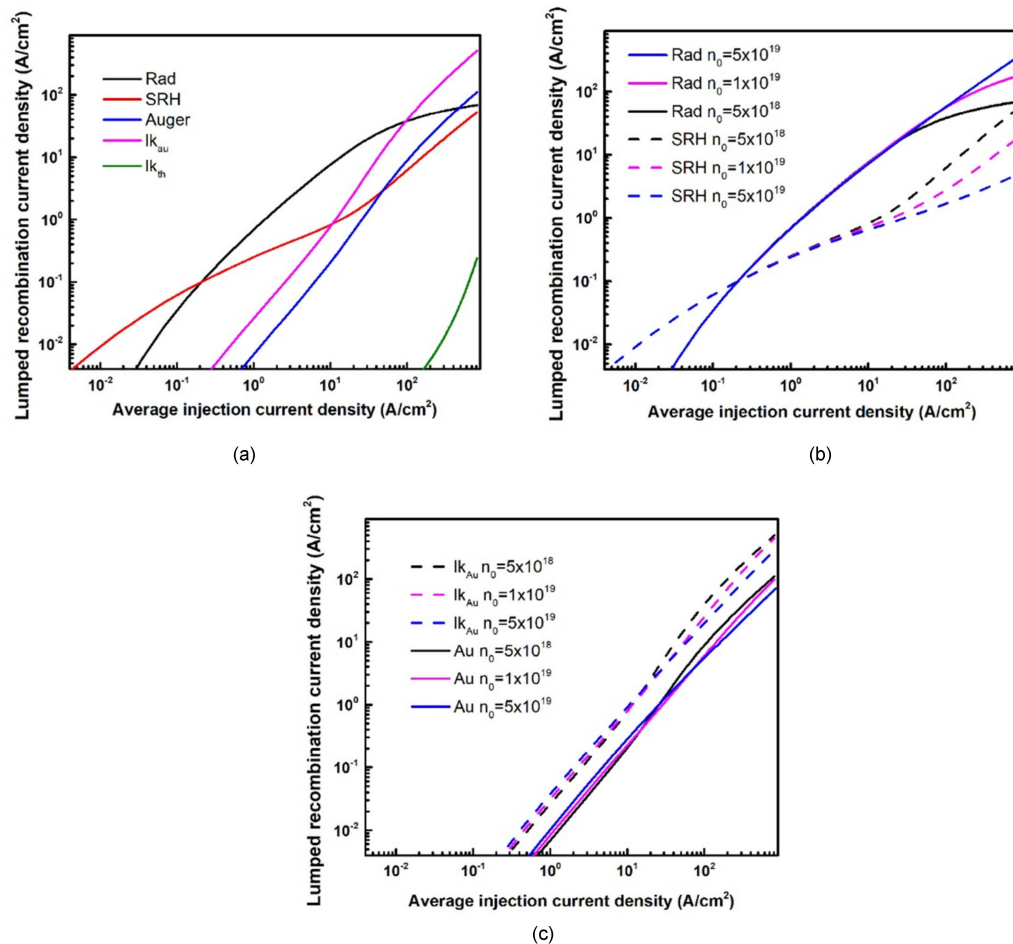


Fig. 6. (a) Lumped recombination current densities versus the various average injection current densities with $n_0 = 5 \times 10^{18} \text{ cm}^{-3}$. “ lk_{Au} ” represents the direct carrier leakage and “ lk_{th} ” is the electron leakage by thermionic emission; (b) and (c) recombination current densities versus various average injection current density and n_0 .

small when the average injection current density is low, as shown in Fig. 5(b). When the average injection current density gets larger, there is a sharp increase. At higher injection levels, the lumped SRH carrier lifetime arrives at a maximum and then decreases as the average injection current density increases. The lumped SRH carrier lifetime rises as the carrier densities increase at a low excitation level, and decreases at a higher one, as confirmed by experimental measurements [30]. The carrier lifetime is shorter when the PSF effect is weaker. Therefore, the lumped carrier density is higher in the structure with the stronger PSF effect, as shown in Fig. 5(a), because it takes much less time for the carriers to decay.

The lumped radiative and Auger coefficients shown in Figs. 5(c) and (d), respectively, decrease with increasing n_0 . As the average injection current density rises, there is a rapid reduction in the lumped radiative coefficient. This is consistent with previous theoretical calculations [41] and experimental measurements [19], [24]. Obviously, there will be a significant decrease in the radiative coefficient in cases where the PSF effect is stronger. The tendency of the average Auger recombination coefficient is similar to that of the average radiative recombination coefficient, for both electron and hole Auger coefficients. At higher injection levels, the Auger coefficient of the electrons decreases more quickly compared to that of the holes, because the electron density increases faster than the hole density, as shown in Fig. 5(a).

Based on the results of the lumped carrier density and the lumped recombination coefficients shown in Fig. 6, the lumped recombination current density of the recombination processes can be calculated. For $n_0 = 5 \times 10^{18} \text{ cm}^{-3}$, the lumped recombination current densities for various average injection current densities are shown in Fig. 6(a). As the average injection current density increases, the lumped recombination current densities for the radiative and non-radiative recombination processes increase due to the increase in the lumped carrier density (Fig. 5(a)). The SRH recombination process is clearly dominant before 0.1 A/cm^2 . From 0.1 A/cm^2 to 40 A/cm^2 , the main contributor to the total recombination process is radiative recombination, with the Auger recombination rate and carrier leakage increasing very quickly. It should be noticed that the lumped direct carrier leakage is dominated by Auger carrier leakage at the active layer rather than electron leakage by thermionic emission at the EBL. The reason for the low electron leakage at the EBL is the high p-doping profile of the LED device examined in this study. After 4 A/cm^2 , the lumped Auger recombination and carrier leakage become larger than the lumped SRH recombination. The magnitude of the lumped direct carrier leakage is higher than the lumped SRH recombination at 10 A/cm^2 and becomes the dominant contributor to the total process after 50 A/cm^2 . At a high injection current density, fast increases of non-radiative recombination processes are observed, while the radiative recombination process slowly increases and saturates. This is indicative of the efficiency droop in LEDs related to non-radiative recombination processes. Although the direct carrier leakage and Auger recombination become the main contributors to the total recombination process at a high injection current density, the average SRH recombination rate still keeps increasing and continues to contribute to the total recombination rate under high injection levels, which is consistent with the predictions in past studies [23], [33].

We investigate the influence of the PSF effect on the recombination processes. The lumped recombination current densities for different average injection current densities, with various n_0 , are shown in Figs. 6(b) and (c). The effect of the PSF on the lumped SRH and radiative recombination current densities is small at low injection levels. The PSF effect has a strong impact on the non-radiative and radiative recombination rates at high injection levels. The lumped recombination current densities for different average injection current densities are plotted in a logarithmic scale. The magnitude of the radiative recombination rate is larger than the magnitude of the SRH rate at a high injection level. It is clear that impact of the PSF effect on the radiative recombination rate is larger than the SRH effect in this regime because radiative recombination has a higher order dependence on the carrier density than on the SRH recombination. The carrier density is significantly affected by the PSF effect at a high injection level, as shown in Fig. 5(a). The stronger PSF effect leads to a higher non-radiative recombination rate and lower radiative recombination rate at higher injection levels. The lumped SRH recombination rate is higher in the case with a stronger PSF effect due to the higher lumped carrier concentration, as shown in Fig. 5(a), while the SRH carrier lifetime is smaller, as shown in Fig. 5(b). The stronger PSF effect may be due to the impurity concentration [28], threading dislocation density, or defect states at the barriers [22] leading to the smaller SRH carrier lifetime. The lumped radiative recombination rate is higher in magnitude in the case with a weaker PSF effect than that with a stronger PSF effect at high injection levels, as shown in Fig. 6(b). Fig. 6(b) shows that the radiative recombination tends to become saturated at high injection levels and the injection current needed to reach the point of saturation is smaller when the PSF effect is stronger. This means that recombination saturation is induced by the PSF effect, which is consistent with the results found in previous studies [20], [24]. The lumped Auger recombination rate and direct carrier leakage are higher in magnitude with a stronger PSF effect, as shown in Fig. 6(c), than for a weaker one at high injection levels due to the higher lumped carrier concentration, as shown in Fig. 5(a).

The distribution of local radiative recombination at the active layer is shown in Fig. 7 for the various average injection current densities and n_0 . It is quite non-uniform at all injection levels. The local radiative recombination distribution is crowded near and under the n-pad due to the effect of current crowding, and it increases in magnitude as the average injection current density rises. The region under the n-pad always has the highest value of radiative recombination as shown in Fig. 7. The distribution of the local radiative recombination is non-circular near the edges due to the limited

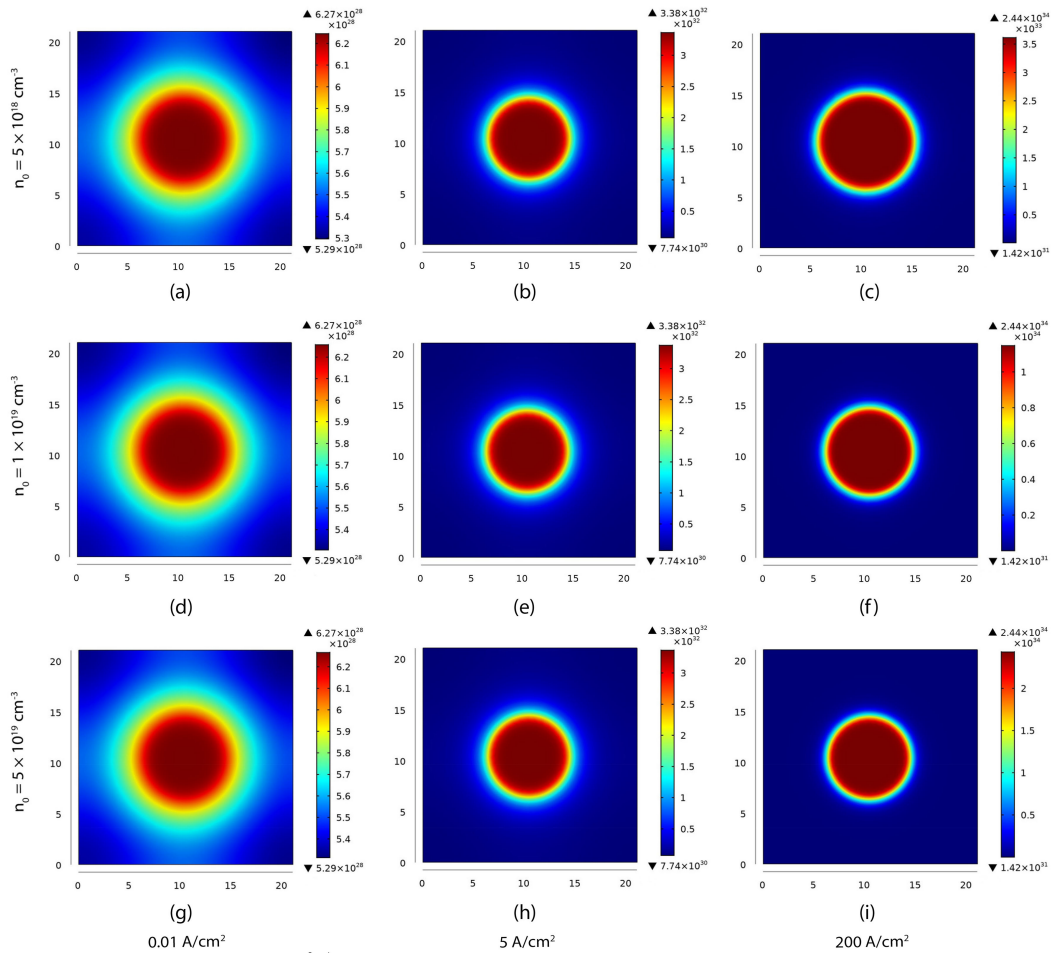


Fig. 7. Local radiative recombination $\text{cm}^{-3}\text{s}^{-1}$ at the active layer with various average injection current densities and n_0 .

length of current spreading and the boundary effect of the square shape of the chip. When the average injection current density is 0.01 A/cm^2 , the area of the higher radiative recombination is concentrated in the region under the n-pad. Since the PSF effect is not significant at small injection currents (Fig. 5(a) and Fig. 6(b)), there is little difference between the maximum and minimum values of radiative recombination at this injection level and the distributions of the radiative recombination in the active layer for different n_0 are quite similar, as shown in Figs. 7(a), (d) and (g). At 5 A/cm^2 , a higher radiative recombination appears in the region under the n-pad with the highest magnitude located at the center. When the average current density is 200 A/cm^2 , a large number of carriers accumulate inside the active layer. Higher radiative recombination also occurs in the region under the n-pad, with the highest magnitude located at the center, as expected from the distribution of the carrier densities (see Fig. 4). The crowding is very severe in comparison with the 0.01 A/cm^2 case. Although the carrier density in the case with a weaker PSF effect is lower, as shown in Fig. 5(a), the local radiative distribution in the active layer is always higher when the PSF effect is weaker, as shown in Fig. 7. The reason is that a higher carrier density leads to higher non-radiative recombination in the case with a stronger PSF. Moreover, the radiative recombination rate is higher for a weaker PSF effect and it reaches saturation later than the case with a stronger PSF effect, as shown in Fig. 6(b).

The local IQE at the active layer is shown in Fig. 8 for the various average injection current densities and n_0 . The distribution is non-uniform. The distribution of the local IQE is non-circular

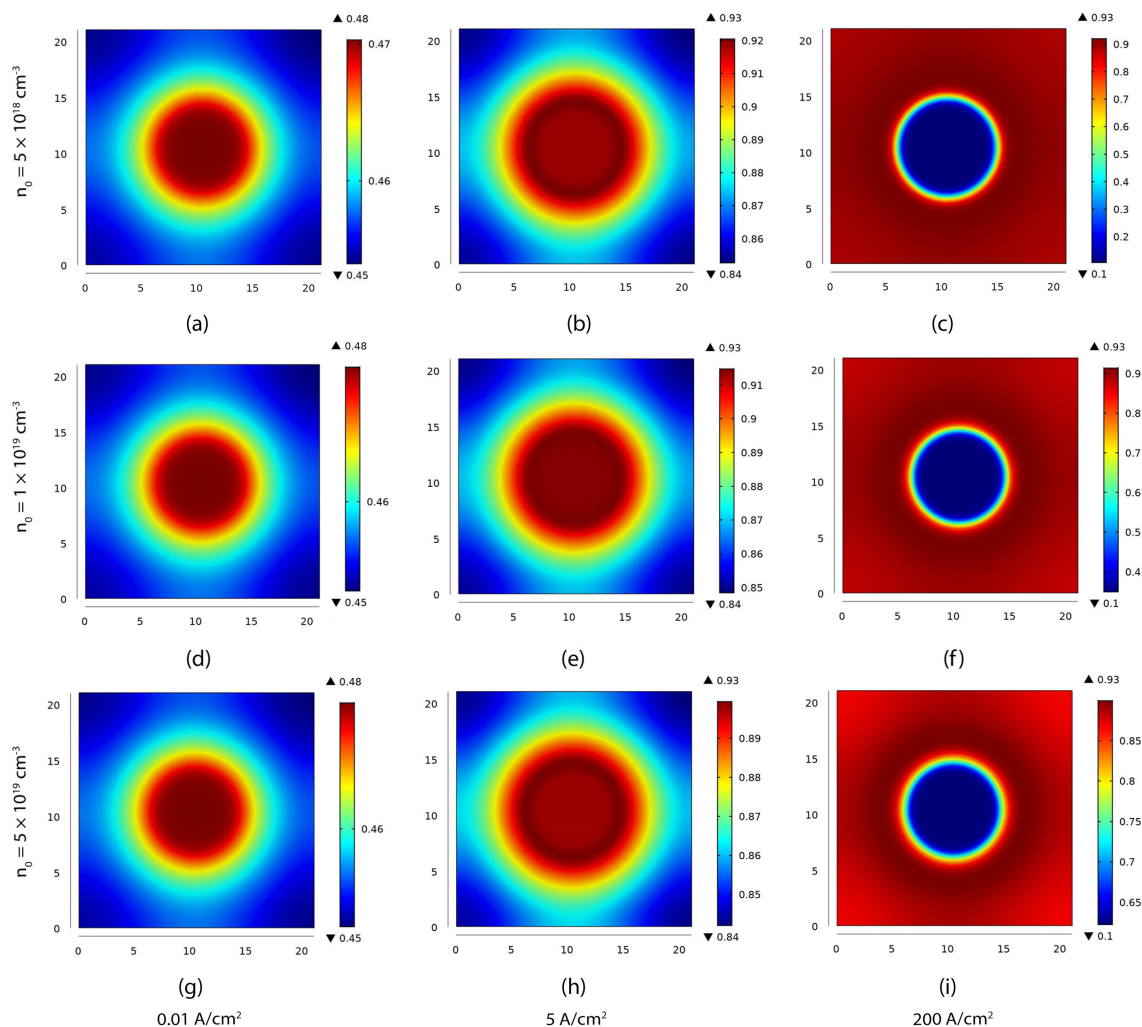


Fig. 8. Local IQE at the active layer with various average injection current densities and n_0 .

near the edges that can be expected from the radiative recombination distribution as shown in Fig. 7. At 0.01 A/cm^2 , a higher local IQE appears in the region under the n-pad, with the highest magnitude located at the center. This can be expected from the radiative recombination distribution (see Fig. 7). The local IQEs at this injection level are similar for different n_0 . When the average injection current density is 5 A/cm^2 , the highest magnitude of local IQE occurs near the edge of the n-pad instead of in the center region. This is due to the increase in the non-radiative recombination which leads to a reduction of the local IQE in the center region. At 200 A/cm^2 , a heavier inversion of the local IQE occurs. The maximum IQE appears near the edge of the n-pad, while the minimum IQE is located at the center. The difference between the maximum and minimum value of the local IQE distribution at this injection level gets larger when the PSF effect is stronger. When the PSF effect is weaker, the distribution is better. The inversion of the local IQE can be explained by the slower rise of the radiative recombination current and the faster increase of the average Auger recombination and leakage current at higher injection levels, as shown in Fig. 6. The region under the n-pad always has the highest value of radiative recombination, as shown in Fig. 7, at any injection current level. However, this does not mean that the local IQE in this region always has the highest value. The value of the local IQE depends on the contributions of the different loss mechanisms and the distribution of the carrier density.

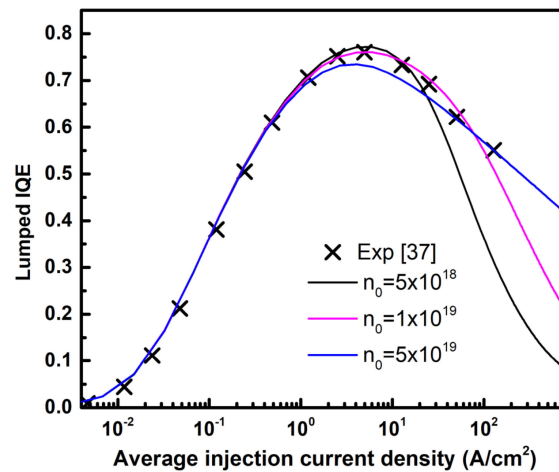


Fig. 9. Lumped IQE versus average injection current density A/cm^2 with various n_0 .

Figure 9 shows the lumped IQE versus the average injection current density A/cm^2 with various n_0 . The efficiency droop can be observed clearly in Fig. 9. As the average injection current density increases, the lumped IQE rises quickly and then drops significantly after reaching the peak value. The peak value is higher when the PSF effect is stronger and the corresponding injection current density is lower. This can be expected due to the higher magnitude of the lumped carrier density in Fig. 5(a). After the IQE reaches its peak value, the radiative recombination current increases slowly and becomes saturated at higher injection levels, while Auger recombination and direct carrier leakage keep increasing until they begin to dominate in the total recombination process, as shown in Fig. 6. The SRH recombination also contributes to the total recombination process at this injection level, as shown in Figs. 6(a) and (b). Therefore, the saturation of the radiative recombination and the increase of the non-radiative recombination rate at high injection levels are the reasons for the efficiency droop in LEDs. The results in Fig. 9 show that, at high injection levels, the efficiency droop is more significant with stronger PSF. This is due to the lower radiative recombination rate and higher SRH recombination, Auger recombination and leakage current, as shown in Figs. 6(b) and (c). The results for the case where $n_0 = 1 \times 10^{19} \text{ cm}^{-3}$ agree well with the experimental measurements [37]. It is obvious that, in the case with stronger PSF, the average IQE decreases more quickly to nearly zero at very high injection levels.

Figure 10 shows the computed current-voltage characteristics. The current-voltage characteristics for the case where $n_0 = 5 \times 10^{18} \text{ cm}^{-3}$ are plotted using both logarithmic and linear scales, while the other ones are plotted only in a linear scale. The current is the result of the voltage drop per the series resistance of all layers in the LED chip. The LED turns on at around 2.9 V and then the voltage drop increases significantly as the injection current increases. The increase in the injection current increases the carrier density and conductivity in the active region. It is found that high injection occurs in the active layer around 3.1 V, where the ideality factor changes from one to two. The I-V curves for different n_0 are similar before 3.1 V as is expected from the similar carrier densities (see Fig. 5(a)) and the recombination processes (see Fig. 6) at low injection levels. In the case with a stronger PSF effect, the LED turns on earlier and the injection current increases more quickly because of the shorter carrier lifetime, as shown in Fig. 5(b) and the higher carrier concentration, as shown in Fig. 5(a). After 3.2 (V), the effect of the PSF on the I-V curve becomes more significant due to the strong recombination processes that occur inside the active layer. The I-V curves shift to the right for higher n_0 . This means that the electrical conductivity in the active layer decrease as the n_0 rises. The LED works at higher applied voltages for a weaker PSF effect.

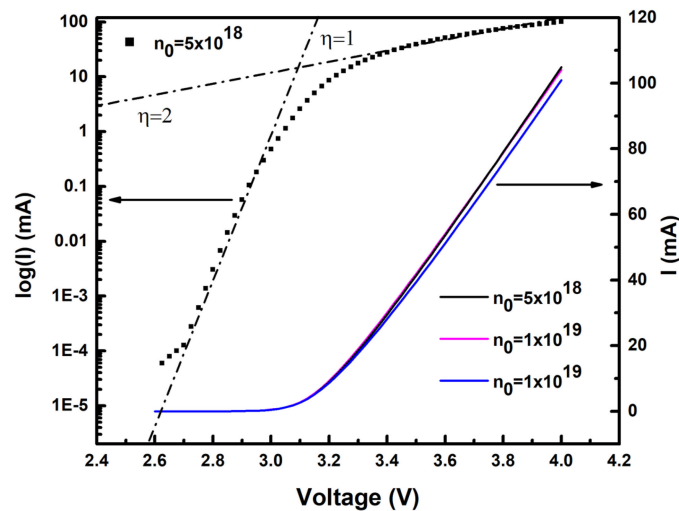


Fig. 10. Computed current-voltage characteristics. The left and right axes are plotted using logarithmic and linear scales, respectively. “ η ” represents the ideal factor.

4. Conclusions

A 3D numerical simulation of carrier transport is conducted to analyze the influence of the PSF effect on the efficiency droop in an SWQ InGaN/GaN LED chip. This modeling process makes it easy to observe the local semiconductor characteristics such as the electron and hole concentrations, the electron current density, the radiative and non-radiative recombination processes, the local IQE and the lumped IQE. A modified formulation for the SRH and the radiative recombination coefficient based on the electron and hole densities and the PSF coefficient is proposed in this study. The behavior of the SRH carrier lifetime is also described with a modified empirical formulation of the SRH. The SRH carrier lifetime increases as the injection current density rises and then starts to drop at a higher injection current density. In the smaller injection current regime, the major contribution to the total recombination process changes from SRH recombination to radiative recombination as the injection current gets larger. On the other hand, the Auger recombination rate and carrier leakage increase quickly. In the higher injection current regime, Auger recombination and carrier leakage become dominant. The variation of the IQE with the injection current is strongly affected by the radiative and non-radiative recombination characteristics. The results show that current crowding always occurs in the region under the n-pad, which leads to non-uniformity in the distribution of the local IQE. The spatial resolution of the IQE in the region under the n-pad is higher in magnitude at a lower injection current density and lower in magnitude at a higher injection current density. The inversion of the local IQE in the region under the n-pad is due to current crowding, which causes the slower rise of the radiative recombination and the faster increase of the non-radiative recombination at higher injection levels. When the injection current becomes larger, the lumped IQE rises rapidly until reaching a maximum and then falls significantly. This is in a good agreement with the experimental measurements [37]. The key factor leading to the droop in the IQE is the faster increase in the Auger recombination and the leakage current that occurs at higher injection levels. The results show that the PSF effect has a strong impact on the IQE behavior of the LED at higher current injection levels. In cases with a stronger PSF effect, the peak value of the lumped IQE is higher in magnitude. The lumped IQE is higher with a weaker effect at higher injection levels. This stronger PSF effect enhances the efficiency droop due to the higher electron concentration and the shorter SRH carrier lifetime. This study shows that in the case where the PSF effect is weaker there is better efficiency at high injection levels, while the case where the stronger PSF effect is better at the injection level when the IQE reaches its peak value. It is obvious that some special design is needed for the shape of the n-pad or electron blocking layer (EBL) to reduce the electron current crowding in the region under the n-pad.

References

- [1] M.-H. Kim *et al.*, "Origin of efficiency droop in GaN-based light-emitting diodes," *Appl. Phys. Lett.*, vol. 91, no. 18, 2007, Art. no. 183507.
- [2] T. Wei *et al.*, "Investigation of efficiency and droop behavior comparison for InGaN/GaN super wide-well light emitting diodes grown on different substrates," *IEEE Photon. J.*, vol. 6, no. 6, Dec. 2014, Art. no. 8200610.
- [3] Y. Shen, G. Mueller, S. Watanabe, N. Gardner, A. Munkholm, and M. Krames, "Auger recombination in InGaN measured by photoluminescence," *Appl. Phys. Lett.*, vol. 91, no. 14, 2007, Art. no. 141101.
- [4] H.-Y. Ryu, D.-S. Shin, and J.-I. Shim, "Analysis of efficiency droop in nitride light-emitting diodes by the reduced effective volume of InGaN active material," *Appl. Phys. Lett.*, vol. 100, no. 13, 2012, Art. no. 131109.
- [5] B. Monemar and B. Sernelius, "Defect related issues in the "current roll-off" in InGaN based light emitting diodes," *Appl. Phys. Lett.*, vol. 91, no. 18, 2007, Art. no. 181103.
- [6] K. Okamoto *et al.*, "Confocal microphotoluminescence of InGaN-based light-emitting diodes," *J. Appl. Phys.*, vol. 98, no. 6, 2005, Art. no. 064503.
- [7] F. Römer and B. Witzigmann, "Effect of Auger recombination and leakage on the droop in InGaN/GaN quantum well LEDs," *Opt. Exp.*, vol. 22, no. 106, pp. A1440–A1452, 2014.
- [8] E. Kioupakis, P. Rinke, K. T. Delaney, and C. G. Van de Walle, "Indirect Auger recombination as a cause of efficiency droop in nitride light-emitting diodes," *Appl. Phys. Lett.*, vol. 98, no. 16, 2011, Art. no. 161107.
- [9] M. Binder *et al.*, "Identification of *nnp* and *npp* Auger recombination as significant contributor to the efficiency droop in (GaIn)N quantum wells by visualization of hot carriers in photoluminescence," *Appl. Phys. Lett.*, vol. 103, no. 7, 2013, Art. no. 071108.
- [10] J. Xie, X. Ni, Q. Fan, R. Shimada, Ü. Özgür, and H. Morkoç, "On the efficiency droop in InGaN multiple quantum well blue light emitting diodes and its reduction with p-doped quantum well barriers," *Appl. Phys. Lett.*, vol. 93, no. 12, 2008, Art. no. 121107.
- [11] J. Liu, J.-H. Ryou, R. Dupuis, J. Han, G. Shen, and H. Wang, "Barrier effect on hole transport and carrier distribution in In Ga N/Ga N multiple quantum well visible light-emitting diodes," *Appl. Phys. Lett.*, vol. 93, no. 2, 2008, Art. no. 021102.
- [12] D. S. Meyaard *et al.*, "Asymmetry of carrier transport leading to efficiency droop in GaInN based light-emitting diodes," *Appl. Phys. Lett.*, vol. 99, no. 25, 2011, Art. no. 251115.
- [13] C.-K. Li and Y.-R. Wu, "Study on the current spreading effect and light extraction enhancement of vertical GaN/InGaN LEDs," *IEEE Trans. Electron Devices*, vol. 59, no. 2, pp. 400–407, Feb. 2012.
- [14] X. Ni *et al.*, "InGaN staircase electron injector for reduction of electron overflow in InGaN light emitting diodes," *Appl. Phys. Lett.*, vol. 97, no. 3, 2010, Art. no. 031110.
- [15] N. Bochkareva *et al.*, "Defect-related tunneling mechanism of efficiency droop in III-nitride light-emitting diodes," *Appl. Phys. Lett.*, vol. 96, no. 13, 2010, Art. no. 133502.
- [16] D.-S. Shin, D.-P. Han, J.-Y. Oh, and J.-I. Shim, "Study of droop phenomena in InGaN-based blue and green light-emitting diodes by temperature-dependent electroluminescence," *Appl. Phys. Lett.*, vol. 100, no. 15, 2012, Art. no. 153506.
- [17] H. Fu, Z. Lu, and Y. Zhao, "Analysis of low efficiency droop of semipolar InGaN quantum well light-emitting diodes by modified rate equation with weak phase-space filling effect," *AIP Adv.*, vol. 6, no. 6, 2016, Art. no. 065013.
- [18] A. David and M. J. Grundmann, "Influence of polarization fields on carrier lifetime and recombination rates in InGaN-based light-emitting diodes," *Appl. Phys. Lett.*, vol. 97, no. 3, 2010, Art. no. 033501.
- [19] P. Tian *et al.*, "Temperature-dependent efficiency droop of blue InGaN micro-light emitting diodes," *Appl. Phys. Lett.*, vol. 105, no. 17, 2014, Art. no. 171107.
- [20] D.-P. Han, J.-I. Shim, and D.-S. Shin, "Analysis of carrier recombination dynamics in InGaN-based light-emitting diodes by differential carrier lifetime measurement," *Appl. Phys. Lett.*, vol. 10, no. 5, 2017, Art. no. 052101.
- [21] J. Hader, J. V. Moloney, and S. W. Koch, "Suppression of carrier recombination in semiconductor lasers by phase-space filling," *Appl. Phys. Lett.*, vol. 87, no. 20, 2005, Art. no. 201112.
- [22] L. Wang *et al.*, "Influence of carrier screening and band filling effects on efficiency droop of InGaN light emitting diodes," *Opt. Exp.*, vol. 19, no. 15, pp. 14182–14187, 2011.
- [23] A. David and M. J. Grundmann, "Droop in InGaN light-emitting diodes: A differential carrier lifetime analysis," *Appl. Phys. Lett.*, vol. 96, no. 10, 2010, Art. no. 103504.
- [24] J. Hader, J. Moloney, and S. Koch, "Beyond the ABC: Carrier recombinations in semiconductor lasers," *Proc. SPIE*, vol. 6115, 2006, Art. no. 61151T.
- [25] R. Ahrenkiel, S. Ahrenkiel, D. Arent, and J. Olson, "Carrier transport in ordered and disordered In 0.53 Ga 0.47 AS," *Appl. Phys. Lett.*, vol. 70, no. 6, pp. 756–758, 1997.
- [26] H. Ryu, K. Jeon, M. Kang, H. Yuh, Y. Choi, and J. Lee, "A comparative study of efficiency droop and internal electric field for InGaN blue lighting-emitting diodes on silicon and sapphire substrates," *Sci. Rep.*, vol. 7, 2017, Art. no. 44814.
- [27] O. Heikkilä, J. Oksanen, and J. Tulkki, "Ultimate limit and temperature dependency of light-emitting diode efficiency," *J. Appl. Phys.*, vol. 105, no. 9, 2009, Art. no. 093119.
- [28] S. Okur *et al.*, "Internal quantum efficiency and carrier dynamics in semipolar (2021) InGaN/GaN light-emitting diodes," *Opt. Exp.*, vol. 25, no. 3, pp. 2178–2186, 2017.
- [29] A. Walker *et al.*, "Nonradiative lifetime extraction using power-dependent relative photoluminescence of III-V semiconductor double-heterostructures," *J. Appl. Phys.*, vol. 119, no. 15, 2016, Art. no. 155702.
- [30] T. Langer *et al.*, "Room temperature excitonic recombination in GaInN/GaN quantum wells," *Appl. Phys. Lett.* vol. 103, no. 20, 2013, Art. no. 202106.
- [31] W. Shockley and W. Read Jr., "Statistics of the recombinations of holes and electrons," *Phys. Rev.*, vol. 87, no. 5, pp. 835–842, 1952.
- [32] R. N. Hall, "Electron-hole recombination in germanium," *Phys. Rev.*, vol. 87, no. 2, p. 387, 1952.

- [33] A. Laubsch *et al.*, "On the origin of IQE-'droop'in InGaN LEDs," *Phys. Status Solidi (c)*, vol. 6, no. S2, pp. S913–S916, 2009.
- [34] M. Deppner, F. Römer, and B. Witzigmann, "Auger carrier leakage in III-nitride quantum-well light emitting diodes," *Phys. Status Solidi, Rapid Res. Lett.*, vol. 6, no. 11, pp. 418–420, 2012.
- [35] K. Chik, "A theoretical analysis of Auger recombination induced energetic carrier leakage in GaInAsP/InP double heterojunction lasers and light emitting diodes," *J. Appl. Phys.*, vol. 63, no. 9, pp. 4688–4698, 1988.
- [36] A. C. Espenlaub, A. I. Alhassan, S. Nakamura, C. Weisbuch, and J. S. Speck, "Auger-generated hot carrier current in photo-excited forward biased single quantum well blue light emitting diodes," *Appl. Phys. Lett.*, vol. 112, no. 14, 2018, Art. no. 141106.
- [37] B. Galler *et al.*, "Influence of indium content and temperature on Auger-like recombination in InGaN quantum wells grown on (111) silicon substrates," *Appl. Phys. Lett.*, vol. 101, no. 13, 2012, Art. no. 131111.
- [38] B. Hahn, B. Galler, and K. Engl, "Development of high-efficiency and high-power vertical light emitting diodes," *Jpn. J. Appl. Phys.*, vol. 53, no. 10, 2014, Art. no. 100208.
- [39] D. J. Griffiths, *Introduction to Electrodynamics*. Englewood Cliffs, NJ, USA: Prentice-Hall, 2005.
- [40] W. Zimmerman, "Experimental verification of the Shockley–Read–Hall recombination theory in silicon," *Electron. Lett.*, vol. 9, no. 16, pp. 378–379, 1973.
- [41] E. Kioupakis, Q. Yan, D. Steiauf, and C. G. Van de Walle, "Temperature and carrier-density dependence of Auger and radiative recombination in nitride optoelectronic devices," *J. Phys.*, vol. 15, no. 12, 2013, Art. no. 125006.
- [42] E. Gaubas and J. Vanhellemont, "Comparative study of carrier lifetime dependence on dopant concentration in silicon and germanium," *J. Electrochem. Soc.*, vol. 154, no. 3, pp. H231–H238, 2007.
- [43] S. Rein, *Lifetime Spectroscopy: A Method of Defect Characterization in Silicon for Photovoltaic Applications*, vol. 489. Berlin, Germany: Springer, 2005, p. 188.
- [44] J. Yang *et al.*, "Emission efficiency enhanced by reducing the concentration of residual carbon impurities in InGaN/GaN multiple quantum well light emitting diodes," *Opt. Exp.*, vol. 24, no. 13, pp. 13824–13831, 2016.
- [45] Q. Dai *et al.*, "Internal quantum efficiency and nonradiative recombination coefficient of GaInN/GaN multiple quantum wells with different dislocation densities," *Appl. Phys. Lett.*, vol. 94, no. 11, 2009, Art. no. 111109.
- [46] X. Meng *et al.*, "Study on efficiency droop in InGaN/GaN light-emitting diodes based on differential carrier lifetime analysis," *Appl. Phys. Lett.*, vol. 108, no. 1, 2016, Art. no. 013501.
- [47] S. Selberherr, *Analysis and Simulation of Semiconductor Devices*. New York, NY, USA: Springer Science & Business Media, 2012.
- [48] W. Liu, R. Butté, A. Dussaigne, N. Grandjean, B. Deveaud, and G. Jacopin, "Carrier-density-dependent recombination dynamics of excitons and electron-hole plasma in m-plane InGaN/GaN quantum wells," *Phys. Rev. B*, vol. 94, no. 19, 2016, Art. no. 195411.
- [49] B.-C. Lin *et al.*, "Hole injection and electron overflow improvement in InGaN/GaN light-emitting diodes by a tapered AlGaIn electron blocking layer," *Opt. Exp.*, vol. 22, no. 1, pp. 463–469, 2014.
- [50] E. F. Schubert, T. Gessmann, and J. K. Kim, *Light Emitting Diodes*. New York, NY, USA: Wiley, 2005.
- [51] J. Piprek, "Efficiency droop in nitride-based light-emitting diodes," *Phys. Status Solidi (a)*, vol. 207, no. 10, pp. 2217–2225, 2010.
- [52] C. K. Sun, S. Keller, G. Wang, M. Minsky, J. Bowers, and S. DenBaars, "Radiative recombination lifetime measurements of InGaN single quantum well," *Appl. Phys. Lett.*, vol. 69, no. 13, pp. 1936–1938, 1996.
- [53] Q. Dai *et al.*, "Carrier recombination mechanisms and efficiency droop in GaInN/GaN light-emitting diodes," *Appl. Phys. Lett.*, vol. 97, no. 13, 2010, Art. no. 133507.
- [54] B. Cao *et al.*, "Effects of current crowding on light extraction efficiency of conventional GaN-based light-emitting diodes," *Opt. Exp.*, vol. 21, no. 21, pp. 25381–25388, 2013.
- [55] A. Zinovchuk, O. Y. Malyutenko, V. Malyutenko, A. Podoltsev, and A. Vilisov, "The effect of current crowding on the heat and light pattern in high-power AlGaAs light emitting diodes," *J. Appl. Phys.*, vol. 104, no. 3, 2008, Art. no. 033115.
- [56] B. Laikhtman, A. Gourevitch, D. Donetsky, D. Westerfeld, and G. Belenky, "Current spread and overheating of high power laser bars," *J. Appl. Phys.*, vol. 95, no. 8, pp. 3880–3889, 2004.